Electrostatically induced mixing in confined stratified multi-fluid systems

Radu Cimpeanu[a], Demetrios T. Papageorgiou[a,*]

[a]*Department of Mathematics, Imperial College London, SW7 2AZ, London, United Kingdom*

Abstract

Electrostatic control mechanisms underpin a wide range of modern industrial processes, from lab-on-a-chip devices to microfluidic sensors for security applications. During the last decades, the striking impact of fluid interface manipulation in contexts such as polymer self-assembly, micromanufacturing and mixing in viscous media has established the field of electrically driven interfacial flows as invaluable. This work investigates electrostatically induced interfacial instabilities and subsequent generation of nonlinear coherent structures in immiscible, viscous, dielectric multi-layer stratified flows confined in channels with plane walls. The present study demonstrates theoretically that interfacial instabilities can be utilized to achieve efficient mixing in different immiscible fluid regions. This is accomplished by electrostatically driving stable flows far from their equilibrium states to attain time-oscillatory and highly nonlinear flows producing mixing. The nonlinear electrohydrodynamic instabilities play the role of imposed background velocity fields or moving device parts in more traditional mixing protocols. Initially, simple yet efficient on-off voltage protocols are investigated and subsequently symmetry-breaking voltage distributions are considered and shown to considerably enhance the achieved level of mixing. Both two and three-dimensional flows, containing realistic fluid configurations (water and oils), are computed using direct numerical simulations based on the Navier-Stokes equations. Such numerical investigations facilitate the quantitative study of the flow into the fully nonlinear regime and constitute the basis of optimization methods in the context of microfluidic mixing applications in two- and three-dimensional geometries.

Keywords: microfluidics, lab-on-a-chip, stability, control, volume-of-fluid method

1. Introduction

Flow control at increasingly small scales is a key challenge in a wide range of fields, from biology, chemistry and medicine to industrial design in electronics, just to name a few examples. Physical interactions in microdevices are very rich, as often multi-physics elements are required to achieve

*Corresponding author
URL: `http://www.imperial.ac.uk/people/d.papageorgiou` (Demetrios T. Papageorgiou)

specialized goals. Gravitational forces are typically negligible at such small scales and the barrier to further reduce the dimensions in applications is a challenge that makes microfluidics one of the most vibrant areas of contemporary research. In multi-fluid flows capillary and viscous forces typically compete to select the dynamics, however external forces such as electric or magnetic fields and even acoustic actuators are becoming increasingly more common in the search for optimal solutions.

Lab-on-a-chip devices, as illustrated in the review of Franke & Wixforth [10], play a primary role in achieving highly efficient solutions for micro scale applications. Such systems have been widely studied theoretically, computationally and experimentally with convincing degrees of success. We refer the reader to the work of Stone *et al.* [33] and the review by Craster & Matar [8] for diverse examples. Of particular relevance is the case of pattern formation from the self-assembly of polymeric liquid films, where microfluidic devices have been critical in the search for techniques to reduce the size of integrated circuit components, as highlighted by Schäffer *et al.* [31].

In the present work we expand on the role of electric field induced dynamics in microchannels. The mechanism is particularly attractive due to the ease of its applicability on the micro scale and its success in achieving control of interfacial fluid motion. It is well known that fields which are parallel to the fluid-fluid interface have a stabilizing role and may be used to prevent interfacial rupture or induce and control a certain behavior within a geometry. The theoretical and computational study of Cimpeanu, Papageorgiou & Petropoulos [6] demonstrates that interfacial oscillations can be sustained in a flow where heavier fluid lies above lighter fluid (the classical problem of the Rayleigh-Taylor instability [27, 35]) so that controlled time-periodic motion is achieved in an otherwise highly unstable system. On the other hand, the pioneering work of Melcher [19, 20] and Taylor & McEwan [36] outlines how electric fields which are perpendicular to the fluid-fluid interface have a destabilizing effect on systems that are stable in the absence of an electric field. An increase in the voltage potential difference produces a stronger instability (expressed via higher growth rates), as well as an increase in the band of unstable modes. The ability to accurately study and harness this process has led to exciting advances in soft lithography, as indicated by Schäffer *et al.* [31]. Theoretically, Ozen *et al.* [24] and Li *et al.* [17] conducted linear and nonlinear stability studies on electrified shear flows, and observed electrically induced interfacial waves. The experimental work of Ozen *et al.* [25] demonstrates the use of electrohydrodynamic instabilities to generate a monodisperse distribution of droplets encapsulated in a second liquid phase in a microchannel - larger applied voltages produce smaller sized droplets. We also mention the feedback control experiments of Melcher & Warren [21], who successfully studied the control of instabilities in a stably stratified air-gas system in a millimeter sized circular device. Moreover, the influence of AC fields has been studied theoretically and has been shown to allow further control of the fluid-fluid interfaces in bilayer and trilayer liquid films - see Roberts & Kumar [28, 29].

As mentioned earlier, in contrast to larger scale hydrodynamics, the salient physics within mi-

crochannels changes significantly. Due to the prominence of viscous forces, the process of mixing becomes very challenging. Fluid mixing of two (or more) species is related to the interspersion of segregated fluid regions. As highlighted in the work of Ottino & Wiggins [23], efficient mixing is vitally related to achieving a large interfacial area between the fluids being mixed, thus facilitating intermolecular diffusion. In small devices turbulence is typically absent and so mixing must rely on diffusion unless the system is subjected to external forces. Furthermore, efficient mixing devices have to reach their targets in a very small amount of space, with minimal energy, and under time constraints in order to be practical. We refer the interested reader to the work of Hessel *et al.* [12] and Suh & Kang [34], who present many useful mixing principles within the context of microfluidic mixing. Small system size presents technological assembly challenges (as well as cost), and very often the actuation needs to be very strong to accurately establish a desired dynamics in the flow. Lee *et al.* [16] have recently reviewed the most popular mixing devices in millimeter and sub-millimeter geometries. It is common to divide mixing into the passive and active categories. Passive mixers often rely on channel geometry to achieve mixing by enhancing molecular diffusion. This is typically accomplished by allowing more time for the flow to diffuse within an intricate network of channels or pre-designed spatial structures. On the other hand, active mixers abandon complex geometries in favor of the use of external forces (such as electricity, magnetism, acoustics or time pulsing). Channels are often simplistic in design and the focus lies in constructing optimal external force fields on the flow.

One of the most studied active devices is the T-mixer. The simple layout allows for extensive experimental explorations and it often offers a straightforward option to incorporate additional effects into the flow. Variations to traditional mixing, including time pulsing, have been explored by Glasgow & Aubry [1] and Goullet *et al.* [11]. El Moctar *et al.* [22] present an extension of the classical T-mixer using electric fields, which is also expanded on in Tsouris *et al.* [39]. The strength of the electric fields involved is most often of order 10^5 to 10^7 V/m, which can easily be achieved by imposing a voltage potential difference of $\mathcal{O}(10^2)$ V across a millimeter sized geometry (or less). Zahn & Reddy [42] present an extension to a T-mixer with three fluid layers and conduct both theoretical and experimental studies with voltage potential differences of up to 9×10^5 V/m.

Here we present a novel approach that introduces an active mixer which does not require an imposed velocity field or any moving parts. We extend the preliminary work of Cimpeanu & Papageorgiou [4] and incorporate the concepts of sustained interfacial oscillations [6] and non-uniform, symmetry-breaking electric field distributions [5] to the advantage of mixing at small scales. The system is driven exclusively by the action of the electric field and we show how efficient mixing can be achieved in practical situations, by modeling real-life fluids in both two-dimensional and three-dimensional geometries.

The structure of the rest of the paper is as follows. Section 2 presents the mathematical model and

outlines the relevant physical quantities and governing equations (subsection 2.1), carries out a linear stability analysis (subsection 2.2), and validates the theory using direct simulations (subsection 2.3) where we elaborate further on the numerical aspects of our work. Section 3 illustrates the effect of simple electric field protocols which are expected to be easy to design in experimental conditions. Two-dimensional (subsection 3.1) and three-dimensional (subsection 3.2) results are presented and the performance of the imposed protocols is assessed using classical molecular diffusion arguments. Conclusions and comments on future work are given in section 4.

2. Mathematical Model

The mathematical model that follows is similar to that presented by Cimpeanu and Papageorgiou [5] in the context of microfluidic pumping, hence the description here will be brief. Consider two incompressible, immiscible and viscous fluids of arbitrary constant densities $\rho_{1,2}$ and constant viscosities $\mu_{1,2}$. The fluids are assumed to be perfect dielectrics and have constant permittivities $\epsilon_{1,2}$ - we assume that there are no impressed charges in the flow. A schematic is provided in Fig. 1. A Cartesian coordinate system is used with the channel walls parallel to the horizontal $x-$axis; the channel has height L and is considered to be sufficiently long - in the numerical work that follows it is reasonable to assume periodic boundary conditions in the horizontal direction. A constant vertical electric field of magnitude $\bar{V}^*/L$ is imposed by a voltage potential difference $\bar{V}^*$ across the channel walls - see Fig. 1.

The interface is denoted by $y = S(x,t)$ and the lower fluid 1 occupies the region $-L/2 < y < S(x,t)$, while the upper fluid 2 occupies the domain $S(x,t) < y < L/2$ (our numerical results capture multivalued interfaces but for clarity we present the model in terms of Cartesian coordinates). We use subscripts $1,2$ to refer to quantities in each corresponding region. An extension to three dimensions, studied at a later stage, is shown in Fig. 1b. All quantities of interest extend naturally and the interface in this case is described by $y = S(x,z,t)$.

Velocity fields and pressures are denoted by $\mathbf{u}_{1,2}$ and $p_{1,2}$, respectively. Surface tension is present with constant coefficient σ and even though we expect gravity to play a negligible role at very small scales, it is nonetheless useful to retain it for generality. It is shown in section 3 using a concrete example, that in the framework of desktop experiments the induced magnetic field is negligible and hence the electrostatic approximation of Maxwell's equations holds. In this limit we have $\nabla \times \mathbf{E}_{1,2} = 0$ and $\nabla \cdot (\epsilon_{1,2}\mathbf{E}_{1,2}) = 0$. The former equation implies that the electric fields can be described in terms of voltage potentials $\mathbf{E}_{1,2} = -\nabla V_{1,2}$, hence the second equation (Gauss's law) shows that away from the interface the voltage potentials satisfy Laplace's equation in each region.

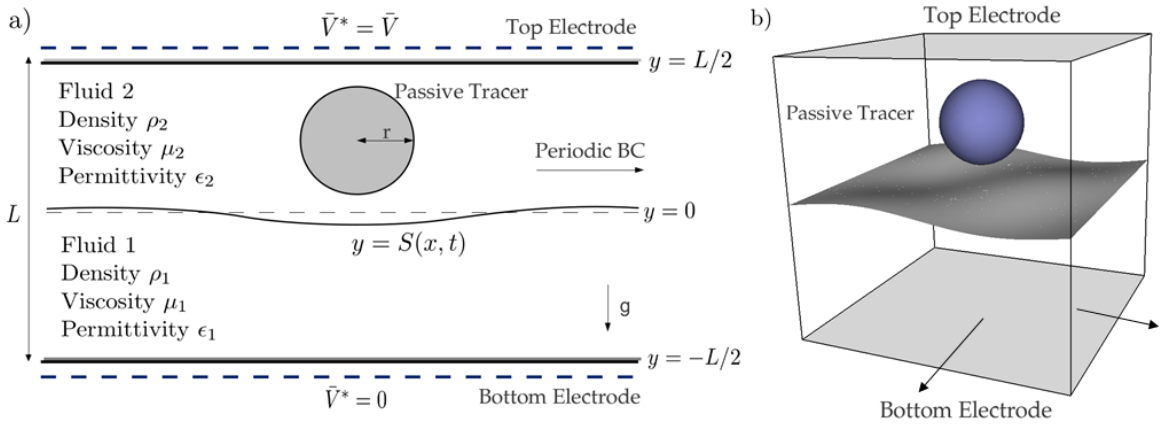

Figure 1: Schematic of the a) periodic two-dimensional and b) doubly periodic three-dimensional domain.

2.1. Problem Formulation

The governing equations are the Navier-Stokes and continuity equations in each phase

$$\rho_1(\mathbf{u}_{1t} + (\mathbf{u}_1 \cdot \nabla)\mathbf{u}_1) = -\nabla p_1 + \mu_1 \Delta \mathbf{u}_1 - \rho_1 g \mathbf{j}, \tag{1}$$

$$\rho_2(\mathbf{u}_{2t} + (\mathbf{u}_2 \cdot \nabla)\mathbf{u}_2) = -\nabla p_2 + \mu_2 \Delta \mathbf{u}_2 - \rho_2 g \mathbf{j}, \tag{2}$$

$$\nabla \cdot \mathbf{u}_{1,2} = 0, \tag{3}$$

with no-slip and impermeability imposed at the walls for $\mathbf{u}_{1,2}$. The Laplace equations for the electric potentials in each fluid are

$$\left(\frac{\partial^2}{\partial x^2} + \frac{\partial^2}{\partial y^2}\right) V_{1,2} = 0. \tag{4}$$

We apply Dirichlet boundary conditions at the walls $y = \pm L/2$ for the potentials,

$$V_1(x, -L/2, t) = 0, \qquad V_2(x, L/2, t) = \bar{V}^*,$$

where $\bar{V}^*$ is a constant. Lorentz forces are absent in the momentum equations due to the constant electrical properties of the perfect dielectrics and the absence of charges in the flow. The coupling between hydrodynamics and electrostatics enters through the nonlinear interfacial boundary conditions. At the sharp interface $y = S(x,t)$ we impose (in order) kinematic conditions, continuity of velocities, continuity of normal and tangential stresses, continuity of the voltage displacement field (Gauss's law),

and continuity of voltage potentials. These are

$$
\begin{aligned}
v_i &= S_t + u_i S_x, \qquad i = 1, 2, && (5)\\
[\mathbf{n}\cdot\boldsymbol{\mathcal{T}}\cdot\mathbf{n}]_2^1 &= \sigma\kappa, && (6)\\
[\mathbf{t}\cdot\boldsymbol{\mathcal{T}}\cdot\mathbf{n}]_2^1 &= 0, && (7)\\
[\mathbf{u}]_2^1 &= 0, && (8)\\
[\epsilon\mathbf{E}\cdot\mathbf{n}]_2^1 &= 0, && (9)\\
[V]_2^1 &= 0, && (10)
\end{aligned}
$$

where $[(\cdot)]_2^1 = (\cdot)_1 - (\cdot)_2$ represents the jump across the interface, $\mathbf{n} = (-S_x, 1)/(1+S_x^2)^{1/2}$, $\mathbf{t} = (1, S_x)/(1+S_x^2)^{1/2}$ are the unit normal and tangent to the interface, respectively, and $\kappa = S_{xx}/(1+S_x^2)^{3/2}$ is the interfacial curvature. The stress tensor $\boldsymbol{\mathcal{T}}$ is given by

$$
\mathcal{T}_{mn} = -p\,\delta_{mn} + \mu\left(\frac{\partial u_m}{\partial x_n} + \frac{\partial u_n}{\partial x_m}\right) + \epsilon\, E_m E_n - \frac{1}{2}\epsilon\,|\mathbf{E}|^2\,\delta_{mn}, \tag{11}
$$

to be evaluated in each fluid region as needed.

To non-dimensionalize we scale lengths by L, velocities by a reference value U (e.g. for capillary scales $U = \sigma/\mu_1$; similarly gravitational or electrical scales can be defined), time by L/U and pressures by $\rho_1 U^2$. The emerging dimensionless parameters correspond to a dimensionless viscosity (inverse Reynolds number), an inverse Weber number, an inverse square Froude number, a voltage scaling, and density, viscosity and permittivity ratios, respectively,

$$
\begin{gathered}
\tilde{\mu} = \frac{\mu_1}{\rho_1 U L}, \quad \tilde{\sigma} = \frac{\sigma}{\rho_1 g L^2}, \quad \tilde{g} = \frac{gL}{U^2}, \quad V^* = UL\sqrt{\frac{\rho_1}{\epsilon_1}},\\
r = \rho_1/\rho_2, \qquad m = \mu_2/\mu_1, \qquad \epsilon = \epsilon_1/\epsilon_2,
\end{gathered} \tag{12}
$$

where ϵ_0 is the permittivity of free space. With $U = \sigma/\mu_1$, we obtain $\tilde{\mu} = O_h^2$, where O_h is the Ohnesorge number. Utilizing these scalings provides the dimensionless system

$$
\begin{aligned}
\tilde{\mathbf{u}}_{1t} + (\tilde{\mathbf{u}}_1\cdot\nabla)\tilde{\mathbf{u}}_1 &= -\nabla\tilde{p}_1 + \tilde{\mu}\Delta\tilde{\mathbf{u}}_1 - \tilde{g}\mathbf{j}, && (13)\\
\tilde{\mathbf{u}}_{2t} + (\tilde{\mathbf{u}}_2\cdot\nabla)\tilde{\mathbf{u}}_2 &= -r\nabla\tilde{p}_2 + m\tilde{\mu}r\Delta\tilde{\mathbf{u}}_2 - \tilde{g}\mathbf{j}, && (14)\\
\nabla\cdot\tilde{\mathbf{u}}_{1,2} &= 0, && (15)
\end{aligned}
$$

where $\mathbf{j} = (0, 1)$, and tildes are used to denote dimensionless quantities. The Laplace equations (4) are unchanged (except for the addition of tildes), and the boundary conditions at the channel walls become

$$
\begin{aligned}
\tilde{\mathbf{u}}_1 = 0, \qquad \tilde{V}_1 &= 0 \qquad \text{at} \qquad y = -1/2, && (16)\\
\tilde{\mathbf{u}}_2 = 0, \qquad \tilde{V}_2 &= \bar{V} \qquad \text{at} \qquad y = 1/2, && (17)
\end{aligned}
$$

where $\bar{V} = \bar{V}^*/V^*$. Boundary and interfacial conditions (5) maintain their form and obtain tilde decorations; the dimensionless stress tensor reads

$$\tilde{\mathcal{T}}_{mn} = -\tilde{p}\delta_{mn} + \tilde{\mu}\left(\frac{\partial \tilde{u}_m}{\partial x_j} + \frac{\partial \tilde{u}_n}{\partial x_m}\right) + \tilde{\epsilon}\tilde{E}_m\tilde{E}_n - \frac{1}{2}\tilde{\epsilon}|\tilde{\mathbf{E}}|^2\delta_{mn}. \tag{18}$$

The well known expression for electrohydrodynamic coupling through the stress tensor (18) has been extensively studied and the reader is referred to Saville [30] for a comprehensive discussion.

2.2. Linear Stability

In what follows we carry out a linear stability analysis (concisely presented, as full details are available in Cimpeanu & Papageorgiou [5]) to determine growth rates in the presence of destabilizing electric fields. Apart from providing a fundamental understanding of the physics of the problem, the results also serve as a basis for comparison and verification of the fully nonlinear computations presented later. The base state solution is given by a flat interface, zero velocities and a uniform vertical electric field in each of the two fluids. A constant undisturbed electric pressure difference at the interface is induced and can be calculated from the normal stress balance to yield

$$p_E = p_2 - p_1 = 2\bar{V}^2\frac{1-\epsilon}{(\epsilon+1)^2}. \tag{19}$$

We linearize the equations and boundary conditions by introducing perturbations

$$\tilde{\mathbf{u}}_{1,2} = \delta\hat{\mathbf{u}}_{1,2}, \qquad \tilde{p}_1 = -\tilde{g}y + \delta\hat{p}_1, \qquad \tilde{p}_2 = -\tilde{g}y/r + p_E + \delta\hat{p}_2, \tag{20}$$

$$\tilde{V}_1 = \frac{\bar{V}}{\epsilon+1}(2y+1) + \delta\hat{V}_1, \qquad \tilde{V}_2 = \frac{\bar{V}}{\epsilon+1}(2\epsilon y+1) + \delta\hat{V}_2, \qquad \tilde{S} = \delta\hat{S}, \tag{21}$$

where $\delta \ll 1$. Normal modes are introduced in the form $\hat{\mathbf{u}}_{1,2}(x,y,t) = \breve{\mathbf{u}}_{1,2}(y)e^{ikx+\omega t} + c.c.$, $\hat{S}(x,t) = \breve{S}e^{ikx+\omega t} + c.c.$, $\hat{V}_{1,2}(x,y,t) = \breve{V}_{1,2}(y)\ e^{ikx+\omega t} + c.c.$, $\hat{p}_{1,2}(x,y,t) = \breve{p}_{1,2}(y)e^{ikx+\omega t} + c.c.$, where $c.c.$ denotes complex conjugates, and the eigenfunctions are determined analytically utilizing the boundary conditions. This leads to a system of homogeneous linear equations for the unknown constants of integration, and a dispersion relation for $\omega(k)$ follows in order to ensure non-trivial solutions (the equation is transcendental and so elementary root finding methods are needed to obtain solutions numerically).

Sample stability results are given in Fig. 2 for increasing values of the imposed electric field $\bar{V}$. In the interest of modeling systems of practical interest, we choose parameters pertaining to a stably stratified two-fluid system of water at 20°C (density $\rho_1 = 998.207$ kg/m^3, viscosity $\mu_1 = 8.95 \times 10^{-4}$ Pa·s and electrical permittivity $\epsilon_1 = 80.4\,\epsilon_0$) and olive oil ($\rho_2 = 918$ kg/m^3, $\mu_2 = 0.081$ Pa·s and $\epsilon_2 = 3.1\epsilon_0$), where $\epsilon_0 = 8.85 \times 10^{-12}$ m^{-3}kg^{-1}s^{4}A^2 is the permittivity of free space; the surface tension between olive oil and water is 0.02 kg $\cdot$ s^{-2}. We use a channel of height $L = 7.5\ mm$ under the action of a gravitational acceleration of 9.80655 m $\cdot$ s^{-2}. Previous work in a similar context, such

as the investigations of Tsouris *et al.* [39] and Zahn & Reddy [42], impose electric field strengths of up to $\mathcal{O}(10^7)$ V/m, which is below the dielectric breakdown limit for common fluids. In Fig. 2 we consider five numerical experiments with voltages ranging from $\bar{V} = 0.1$ to $\bar{V} = 0.5$ non-dimensionally, corresponding to 2×10^6 V/m up to 10^7 V/m.

We are interested in the effect of the electric field on the instability, and expect an increase in growth rates and a widening of the band of unstable modes as the electric field strength increases. This is indeed the case as seen in Fig. 2; for low values of $\bar{V} = 0.1$, 0.2 for example, a small band of long waves are unstable and the size of the band increases (shorter waves becoming unstable) as $\bar{V}$ is increased. Fig. 2 also includes results from direct numerical simulations starting from small initial conditions where linear theory holds, and agreement between analysis and computation is excellent. We elaborate on this aspect in the following subsection.

2.3. Computational Capabilities and Validation

Our numerical methods are based on a volume-of-fluid platform adapted from the Gerris suite of algorithms, constructed by Popinet [26]. We also use the electrohydrodynamics module available in the code architecture and expanded upon by López-Herrera *et al.* [18]. Adaptive meshing and accurate multiphase fluid representation are some of the features that make the computational platform highly suitable for our study. We also mention the extensive numerical studies of Bagué *et al.* [2], López-Herrera *et al.* [18] and references therein, validating and extending the implementation, as well as directing the modules to concrete applications of interest.

One of the essential features is the representation of physical quantities in the region containing the fluid-fluid interface. The density $\tilde{\rho}$ is written in terms of a volume fraction $\mathcal{C}(\mathbf{x}, t)$ as

$$\tilde{\rho}(\mathcal{C}) \equiv \mathcal{C}\tilde{\rho}_1 + (1 - \mathcal{C})\tilde{\rho}_2, \tag{22}$$

where $\tilde{\rho}_1$ and $\tilde{\rho}_2$ are the constant values of the density in the two phases of the flow field. The general density equation is transformed to a volume fraction equation

$$\mathcal{C}_t + \nabla \cdot (\mathcal{C}\tilde{\mathbf{u}}) = 0, \tag{23}$$

and once this is solved for $\mathcal{C}$ the density follows from (22). Viscosity and permittivity differences between phases are treated in an analogous way. In particular, the algorithm incorporates smooth independent variations of ϵ across the thin interface region, with well studied specialized interpolation techniques, as discussed in Tomar *et al.* [38]. The electrostatic potential (in the absence of impressed charges as is the case here) satisfies elliptic equations of the form $\nabla \cdot (\tilde{\epsilon} \nabla \tilde{V}) = 0$, that reduce to Laplace equations away from the interface where the permittivity is constant. We solve for $\tilde{V}$ throughout the domain since $\tilde{\epsilon}$ is known from an equation analogous to (22). The electrostatic forces in the bulk can

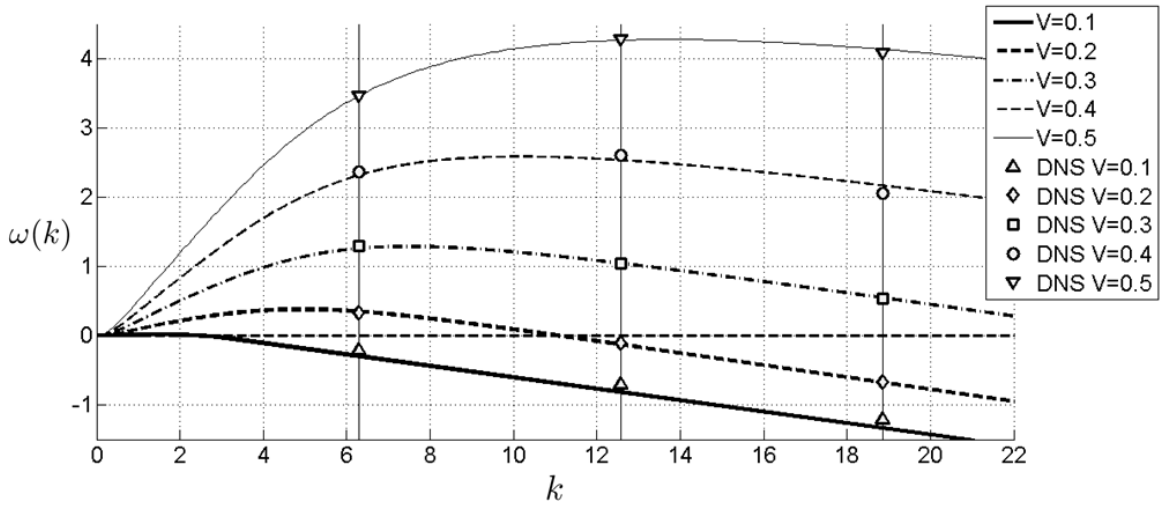

Figure 2: Growth rates $\omega(k)$ illustrating the effect of increasing voltage potential difference $\bar{V}$ on the instability.

be found from taking the divergence of the Maxwell stress tensor - see (18) - and this yields

$$\mathbf{F}_e = -\frac{1}{2}|\tilde{\mathbf{E}}|^2 \nabla \tilde{\epsilon}. \tag{24}$$

These forces are zero away from the interface as expected.

The symbols in Fig. 2 were calculated from direct numerical simulations using Gerris, with fluid parameters corresponding to a water-olive oil system. The initial perturbation of the fluid-fluid interface is described by

$$S(x,0) = A_i \cos(2q\pi x), \tag{25}$$

where q is a positive integer and A_i is the perturbation amplitude, selected to be of $\mathcal{O}(10^{-3})$ and hence within the realm of linear theory initially, allowing the flow to evolve for sufficiently long times prior to reaching the nonlinear regime. To quantify the interfacial dynamics we track the position of several points on the interface throughout the simulation and use a sliding least squares method to extract the relevant growth rates. Thus, the linear regime can be evaluated accurately by reconstruction of the linear dispersion relation as shown by the excellent agreement in Fig. 2. This validation underpins numerical experiments into the nonlinear regime enabling the exploration of efficient microfluidic mixing. Knowing the most unstable wavenumber for a given electric field strength and fluid parameters, we tailor the electric field to allow the manipulation of the dynamics within the confined geometry. In the next section we illustrate how this information can be used to sustain oscillations that lead to enhanced mixing in this class of problems.

3. Results

In this section we present numerical results that show how time varying electric fields can be used to achieve mixing by nudging nonlinear interfacial oscillations that would be absent if the field is switched and kept off. In subsection 3.1 we propose a set of time varying electric fields to be used in this context, and also analyse their performance with regards to mixing efficiency.

3.1. Two Dimensional Flows

3.1.1. On-off time variations in the electric field

We begin by considering simple on-off time variations for the applied electric field, noting that the applied electric field is constant over the channel during the on stage. During the on stage the electric field is above the critical value predicted by linear theory and if it is kept on, the interface generically undergoes nonlinear growth and eventually touches one of the walls in finite time. Hence, we switch the electric field off before touchdown and allow the interface to relax towards its base state solution (this is possible due to the presence of viscosity and the stable stratification of the flow). This procedure is repeated to sustain interfacial oscillations in the flow that in turn induce time oscillatory velocity fields. Such electrostatic forcing was considered by Cimpeanu & Papageorgiou [4] and salient results are reviewed in order to set the stage for more inducing mixing for realistic fluids and particularly the need for electrophoretic forcing considered in section 3.1.2.

Six on-off electric field protocols are considered as shown in Fig. 3. The shaded regions indicate the time intervals during which the electric field is turned on inducing a vertical electric field. For this set of numerical experiments we use parameters (recall (12) for definitions) $r = 6$, $m = 0.25$, $\epsilon = 2$, $\tilde{\mu} = 0.1$ and $\tilde{\sigma} = 0.5$, and a prescribed voltage potential difference $\bar{V} = 15.0$ (these parameters pertain to a system of size $L = 1.9$ mm, and a total duration of approximately 0.3 s). Fluid 1 is chosen to be a typical oil (e.g. olive oil); the density, viscosity and permittivity ratios are of $\mathcal{O}(1)$ providing a wide range of choices for the second fluid - specific water-oil systems are considered later in section 3.1.2. From a computational perspective it is preferable to have a strong density contrast in order to facilitate faster relaxation of the interface towards its flat state when the electric field is switched off.

Our model uses the electrostatic assumption and in what follows we provide a justification of its validity for time-dependent fields (see also Conroy *et al.* [7]) and in particular the absence of induced magnetic fields of any relevance. The magnetic induction equation is given by

$$\nabla \times \mathbf{H} = \mathbf{J} + \epsilon \frac{\partial \mathbf{E}}{\partial t}, \tag{26}$$

where $\mathbf{H}$ is the magnetic field and $\mathbf{J}$ is the current. By construction, the electric field is scaled by $E_0 \sim \bar{V}^*/L$ and we write $\mathbf{H} = H_0\mathbf{H}'$. The frequency Ω with which the electric field is switched on and off reflects the time-dependent element in the voltage model. Using the induction equation (26)

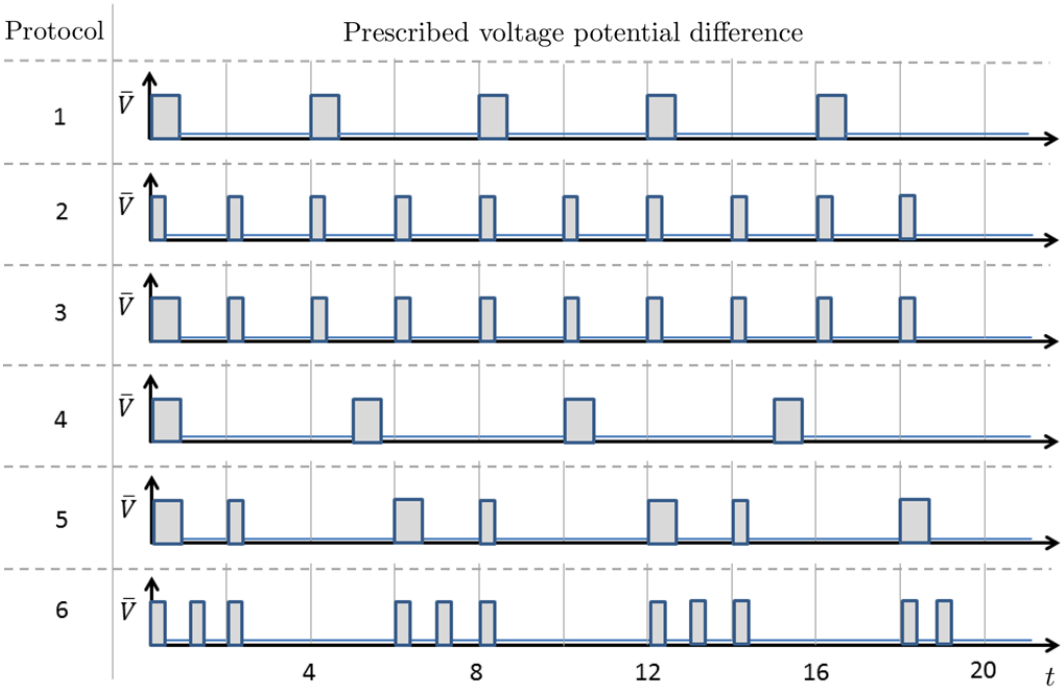

Figure 3: The time variation of each of the six imposed on-off protocols; shaded regions represent the times when the electric field is kept on with a constant voltage that enables the destabilization of the fluid-fluid interface.

yields $H_0 \sim \epsilon_0 E_0 L\Omega$. Consider approximations $\epsilon_0 \sim 10^{-11}\ F\ m^{-1}$, $L \sim 10^{-3}\ m$ and typical electric field strength $E_0 \sim 10^{6-7}\ V\ m^{-1}$. This results in H_0 being at most $H_0 \sim 10^{-7}\Omega\ T\,s$, measured in an appropriate timescale $1/\Omega$, where T denotes teslas and s seconds. Based on an appropriately defined timescale, the duration of the proposed experiment is approximately 1.38 s. With at most 8 on-off switches (evenly distributed in time) this implies $\Omega \sim \mathcal{O}(10^{-1} - 10^{0})$ Hz, and hence $H_0 \approx 10^{-7}\ T$, i.e. the contribution of the magnetic field is negligible. Even in the kilohertz range, the induced magnetic field would still be negligible.

We quantify mixing via numerical experiments in the following manner. A droplet of dimensionless radius $r_d = 0.15$ is introduced in the upper fluid within our computational domain as sketched in Fig. 1. The droplet has the same properties as the upper fluid and represents a region occupied by a passive scalar (a dye, for example) at the initial time. By observing the concentration field c of this passive tracer in time, we deduce the level of mixing induced by the action of the electric field and resulting hydrodynamics. Sample evolutions of the passive tracer field are produced in Fig. 4, where protocols 3 and 5 are shown at different times of the simulation. We note that numerical artifacts in the passive tracer advection lead to minor breaches through the interface (observable in Fig. 5); a careful study reveals that this does not affect the calculated degree of mixing, since the amount of dyed fluid outside the desired region is negligible and this numerical process is restricted to the passive tracer, computed by approximating the velocity field. Furthermore, stringent error tolerances and increased grid refinement levels can be imposed to completely eliminate such effects, but we did not undertake such computations due to the high cost involved.

To quantify the mixing efficiency we follow the ideas of Glasgow & Aubry [1] who propose a measure of mixing in the case of a T-mixer with time pulsing, which also accounts for non-uniform mass flow rate within the channel. In our case there is no background velocity field and hence the quantification of Jha *et al.* [15] is suitable. Briefly, the mixing index $\chi(t)$ is defined by

$$\chi(t) = 1 - \frac{\beta^2(t)}{\beta^2_{\max}}, \tag{27}$$

where $\beta^2 \equiv \langle c^2 \rangle - \langle c \rangle^2$; here $\langle \cdot \rangle$ denotes spatial averaging over the domain, while $\beta^2_{\max}$ is the variance of the fully segregated state. A variance-based indicator is a natural candidate for assessing mixing quality, due to the direct comparison to the perfectly mixed state. Several other mathematical properties of this index, as well as other specialized alternatives, are highlighted by Thiffeault [37]. Inspecting equation (27) we notice that $\chi(t)$ varies from 0 in a fully unmixed regime up to 1 for perfect mixing. In an ideal situation a fully mixed state is described by a constant concentration which is equal to the ratio of the area of the initial passive scalar to the total area of the domain which is the area of region 2 in our case. Fig. 5 shows the evolution of the mixing index $\chi(t)$ for each of the six protocols introduced in Fig. 3. It can be seen from our results that efficient mixing usually occurs when a strong

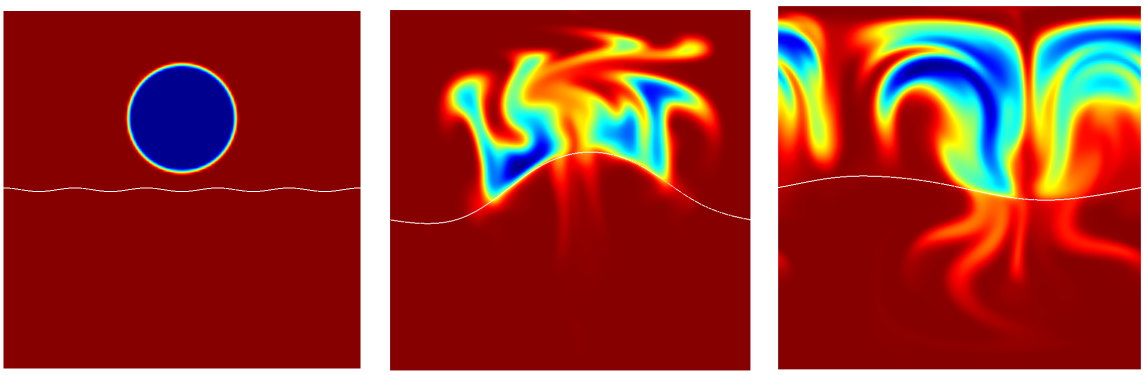

(a) Protocol 3, $t = 0.0$. (b) Protocol 3, $t = 10.0$. (c) Protocol 3, $t = 20.0$.

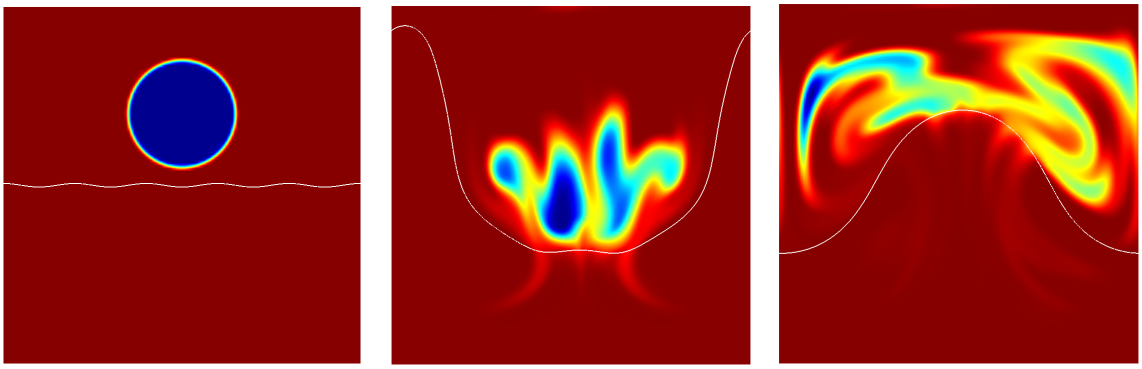

(d) Protocol 5, $t = 0.0$. (e) Protocol 5, $t = 10.0$. (f) Protocol 5, $t = 20.0$.

Figure 4: The passive tracer field (background) and fluid-fluid interface (highlighted in white) under the action of protocol 3 (top) and protocol 5 (bottom) from Fig. 3 at three different times: $t = 0.0$ (left), $t = 10.0$ (center) and $t = 20.0$ (right). The succession of plots shows the gradual mixing of the passive tracer due to the hydrodynamics induced by the electric field. An animation for each of the six on-off protocols is available as electronic supplementary material.

destabilizing electric field persists for a moderate amount of time, so that the interface is close to reaching the channel walls during its unstable cycle. After this initial spreading has occurred, successive on-off switches of short duration are found to sustain interfacial oscillations and lead to highly efficient mixing, with indexes exceeding 0.7. The results presented in Fig. 5 (a subset of which are illustrated in Fig. 4) compete well with previous state-of-the-art examples of both passive and active micromixers, as highlighted in the review of Hessel *et al.* [12] or in the particular cases of Bhagat *et al.* [3], Wang *et al.* [40] and Hossain and Kim [14]. In the aforementioned studies (and numerous others), the devices considered reach mixing indexes of up to $0.5 - 0.6$ (using similar performance measurement methods). Fig. 5 shows that the best mixing is obtained for protocol 3, which achieves a mixing efficiency of over 0.9. We have not addressed the problem of optimal mixing, for example what electric field variations would one need to achieve optimal mixing in a given time, however our results form the basis of such investigations.

The level of improvement in mixing is also quantified by comparing the results to molecular diffusion. Using Fick's law in two dimensions, the mean radius of a diffusing passive scalar droplet in two dimensions, is given by $s \sim \sqrt{4Dt}$, where t is dimensional time and D is the self-diffusion coefficient. For standard fluids (including the ones here), $D = \mathcal{O}(10^{-12} - 10^{-9})$ - see, for example, the experiments of Holz *et al.* [13] and Denkova *et al.* [9]. A straightforward approximation with a value of $D = 10^{-10}\ m^2\ s^{-1}$ amounts to an average spread of $s \sim 1.09 \cdot 10^{-5}\ m$ in the time frame of the numerical experiments in the $1.9 \times 10^{-3}\ m$ channel; this is seen to be two orders of magnitude lower than the mean particle displacement under the action of electrohydrodynamic mixing. The evolution of the mixing index solely via molecular diffusion has been computed for reference (see Fig. 5) and evolves from 0.0369, the starting value given by the discretization of the concentration field, to 0.0377 by the end of the runs.

3.1.2. Water-oil systems: On-off and dielectrophoresis-inducing voltage protocols

In this section we present computations for water-oil systems. The relevant dimensionless parameters in this case are $r = 1.0837$, $m = 90.5027$, $\epsilon = 25.9354$, $\tilde{\mu} = 4.4082 \times 10^{-4}$, and $\tilde{\sigma} = 0.0363$. As mentioned earlier such computations are challenging particularly due to the relatively slow relaxation of the interface to its initial position during times when the field is switched off.

After extensive numerical experimentation we concluded that good mixing results can be achieved in this case if in addition to switching the field on-off, the imposed voltage at the upper electrode also has a spatial variation that is linear in x (such non-uniform voltages were imposed by Yeo *et al.* [41] in their study of electrophoretically induced droplet splitting and by Singh & Aubry [32] in the context of droplet translation in microdevices). More precisely we impose the following voltage at the upper

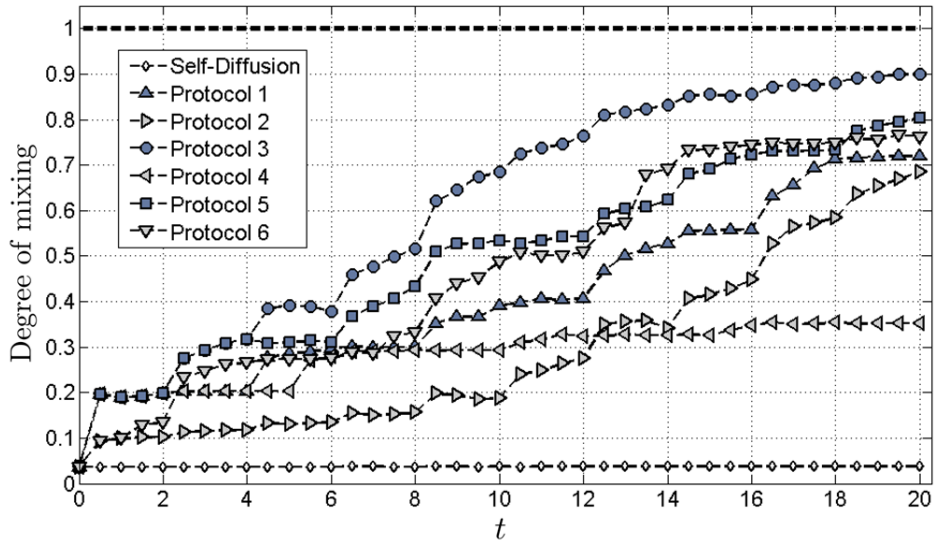

Figure 5: Evolution of mixing index $\chi(t)$ under the action of the six selected on-off protocols presented in Fig. 3.

electrode $y = L/2$

$$V_2(x, L/2, t) = \begin{cases} C + Ax + \dfrac{A}{2}\left(-\dfrac{2}{\pi}\tan^{-1}(\delta'(x+0.5)) - \dfrac{2}{\pi}\tan^{-1}(\delta'(x-0.5))\right) \text{ if } t_{\text{on}}, \\ 0 \text{ if } t_{\text{off}}. \end{cases} \tag{28}$$

In (28) the parameters t_{on} and t_{off} measure the times when the voltage is on or off, respectively. Also, C is a constant and for all the experiments in this subsection it is taken to be 0.3 (this value corresponds to the third curve in Fig. 2). The contribution Ax introduces dielectrophoretic effects into the model with strength measured by A. The trigonometric terms in equation (28) are used to produce a smooth transition at the edges of the domain $x = \pm 1/2$ so that $V_2(x, L/2)$ is a smooth spatially periodic function; the parameter D describes the sharpness of this transition with larger values of D producing sharper transitions - we use $D = 50$ in all our numerical experiments. The voltage on the lower electrode remains fixed at 0, such that $V_1(x, -L/2, t) = 0$ for all t.

We construct a series of nine runs spanning over 50 dimensionless time units. The first run is a control with the field switched off and the passive scalar allowed to spread under molecular diffusion. All subsequent cases represent scenarios in which the electric field is switched on at the start of the simulation and the interface is allowed to grow until it is in close proximity to the wall. We wish to prevent wall touchdown (the topological transition is unlikely to be beneficial to mixing, and also such phenomena are beyond the scope of the present computational study) and so switch the electric field off, thus prompting the relaxation to a flat interfacial position. The relaxation time t_{off} from near the wall towards the base state is considerably larger than the time t_{on} taken by the interface to reach

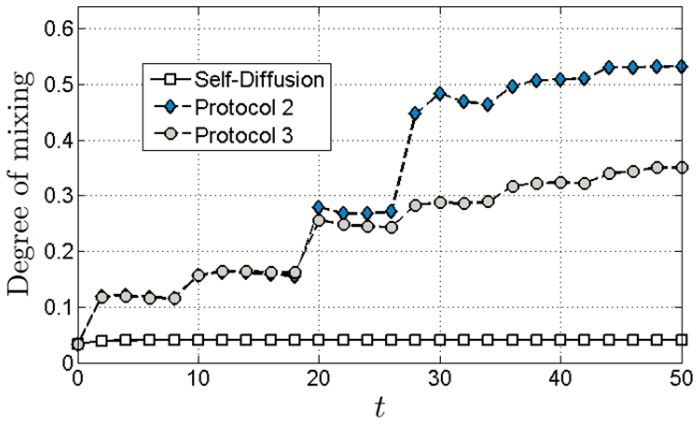

Figure 6: Evolution of the mixing index $\chi(t)$ for the best performing on-off protocols. The two examples have on-off cycles of 9 dimensionless time units; $A = 0.05$ for protocol 2 and $A = 0.1$ for protocol 3. All numerical experiments use $C = 0.3$ and $\delta' = 50$ - see equation 28 for the imposed voltage at the upper wall.

the walls. By allowing for successive relatively short on intervals long off intervals, we find that the induced hydrodynamics produce strong mixing.

The relevant computational parameters that remain in equation (28) are the parameter A measuring the horizontal voltage non-uniformity, and the times t_{on} and t_{off}. We considered two families of tests with four subcases each (defined by $A = \{0.0, 0.05, 0.1, 0.2\}$), in addition to the non-electrified control experiment. The first set of tests has $t_{\text{on}} = 0.65$, followed by relaxation periods t_{off} of 8.35 dimensionless time units. Thus we use cycles of 9 dimensionless units that run in sequence until the maximum time of 50 units is reached, for each value of A starting from 0 corresponding to constant voltage, and increasing thus imposing stronger directionality in the flow. This is desirable since it introduces a break in symmetry that significantly enhances mixing. The second test covers the same range of values in A, however the on-off cycle is different and is described by $t_{\text{on}} = 0.3$, followed by smaller relaxation periods $t_{\text{off}} = 5.7$ units, i.e. introducing cycles of total duration of 6 time units.

Before presenting results we emphasize that this is a more difficult system to work with due to the values of density, viscosity and permittivity ratios that make it challenging to achieve good mixing due to unwanted nonlinear phenomena that can emerge, such as interfacial wall touchdown and topological transitions. In addition, other protocols can lead to the mixing index χ reaching a small value plateau due to interface flattening which is undesirable for mixing. In Fig. 6 we illustrate results for the successful protocols 2 and 3, along with the self-diffusion case which is seen as the bottom curve with white squares - it attains a mixing index of approximately $\chi = 0.037$. Based on molecular diffusion arguments we can estimate the average spread of the passive scalar to be $s \sim 2.35 \times 10^{-5}\ m$. On the

other hand, protocols 2 and 3 show a marked improvement of the mixing index, becoming larger than 0.5 in the former case. In all cases, there is a sensitivity in the dynamics that we wish to highlight. As mentioned above, when wall touchdown occurs the simulation is interrupted - protocols 1 and 7 are such examples that are terminated after $t = 30 - 35$ units. On the other hand, if the overall action of the electric field is too weak it then allows a full relaxation of the interface without generating instability and sustained oscillations of sufficiently high amplitude to have a visible effect on mixing - such is the case for protocols 4 and 8, where $A = 0.2$. The reason for this is that with $A = 0.2$ the voltage potential (see (28)) varies between 0.1 and 0.5 and so a relatively weak field acts on the left of the domain - contrast this with $A = 0$, for example, when a larger uniform field would be acting there. We observe that the even though the horizontal distribution of the voltage at the upper wall steers the interface towards the edges of the domain through a displacement of equipotential lines, the interval t_{on} is too small to induce a large interfacial displacement, and the subsequent relaxation returns the interface to its flat base state. Further cycles have little effect in the area outside the immediate vicinity of the fluid-fluid interface leading to diffusion with a modest evolution of the mixing index in time. The parameters can be optimized to overcome these shortcomings, however it is important to underline their significance and physical effects on the flow. With appropriately tuned values for A and t_{on}-t_{off} cycles, desirable results are found for protocols 2 and 3 as shown. We also point out that protocols 1 and 5, which have $A = 0$ and coincide with the constant voltage scenarios, are not as successful as their non-uniform counterparts. We conclude that an optimization procedure would produce significant improvements and perhaps a feedback control mechanism that adapts to flow conditions (interfacial position in the domain) in the selection of t_{on} and t_{off} would be beneficial and a possible future step in this study.

To conclude, efficient mixing occurs when a strong destabilizing electric field persists for a moderate amount of time, such that the fluid-fluid interface gets close to the channel walls. After the initial spreading has occurred, successive on-off switches of appropriately chosen intervals in time, sustain interfacial oscillations and generate mixing with indexes exceeding 0.5 in a very short timescale. In the following subsection we explore similar mixing mechanisms in three dimensions.

3.2. Mixing in Three Dimensional Flows

The two-dimensional results described above have been extended to three dimensions in order to investigate mixing for single or multiple droplets of passive scalars. A doubly periodic (in $x-$ and $z-$directions) domain is used between two solid wall electrodes at $y = -L/2$ and $y = L/2$ (in dimensional terms). As established already, the electric field perpendicular to the fluid-fluid interface has a destabilizing effect and we use on-off protocols with both uniform and non-uniform voltage potential distributions in order to generate efficient mixing within such a geometry. The imposed

voltage at the upper wall is taken to be

$$V_1(x,-L/2,z,t) = \begin{cases} C + Ax + \dfrac{A}{2}\left(-\dfrac{2}{\pi}\tan^{-1}(\delta'(x+0.5)) - \dfrac{2}{\pi}\tan^{-1}(\delta'(x-0.5))\right) \text{ if } t_{\text{on}}, \\ 0 \text{ if } t_{\text{off}}, \end{cases} \tag{29}$$

and this is a straightforward extension of condition (28) used for two-diemensional flows, but now we impose a non-uniform voltage on the lower wall (mixing is tracked in the lower fluid now). We have chosen to model a spherical drop of dimensionless radius $r_d = 0.15$ in the bottom fluid (mostly for better visualization reasons). We select one uniform electric field case ($A = 0.0$) and contrast it to a regime with a moderate value $A = -0.1$ - the non-zero value of A was chosen so as to prevent wall touchdown but still allow for symmetry-breaking effects.

Due to the complexity of the three-dimensional setup and in the interest of computational efficiency, we did not use the exact water-oil parameters described in section 2. In particular we changed the density ratio of the two fluids to be $r = 6$. Such a more stably stratified system leads to faster relaxation times during t_{off}, and this considerably improves computational runtimes. Secondly, we altered the dimensional height of the domain from $L = 7.5\ mm$ to $L = 25\ mm$. These alterations do not interfere with the physical mechanisms involved and have been introduced strictly for numerical reasons. The duration of the numerical experiments in physical time is approximately $0.5\ s$.

The results of utilizing a uniform voltage potential distribution are presented in Fig. 7 (a)-(c), which illustrates the time evolution of the concentration isocontour having a value equal to the target concentration value in the problem, i.e. the constant obtained by dividing the volume of the sphere into half of the volume of the box domain (the passive tracer is restricted to the region occupied by fluid 1). In addition, the plots present the pressure field at the cross-section $z = -0.2$, with red color-coding denoting high pressures (bottom of the container) and blue denoting low values (top of the container), along with the computational mesh at that particular time - the mesh is seen to be heavily refined around the interface (depicted by a dark curve) between the fluids. We notice a progressive modification of the drop shape and this provides a strong indication of mixing in the flow. We turn again to the efficiency evaluation against molecular self-diffusion by comparing the average theoretical spread under diffusion with paths of individual particles in the simulated flow. To this end, in Fig. 7 (d)-(e), we marked four particles that were positioned on the surface of the spherical drop at $t = 0.0$. Note that a significantly higher number of such Lagrangian particles was tracked and analyzed statistically, however for visualization purposes we illustrate results for the four particles included in Fig. 7. For reference we note that in the same time frame as the simulations, the root mean square distance of the particles with a self-diffusion coefficient of $D = 10^{-10}\ m^2/s$ is $1.73 \times 10^{-5}\ m$. This is well below (two orders of magnitude or more) the distances traversed by the tracked particles in our $\mathcal{O}(10^{-2})\ m$ sized domain. We observe significantly improved results when comparing to molecular self-

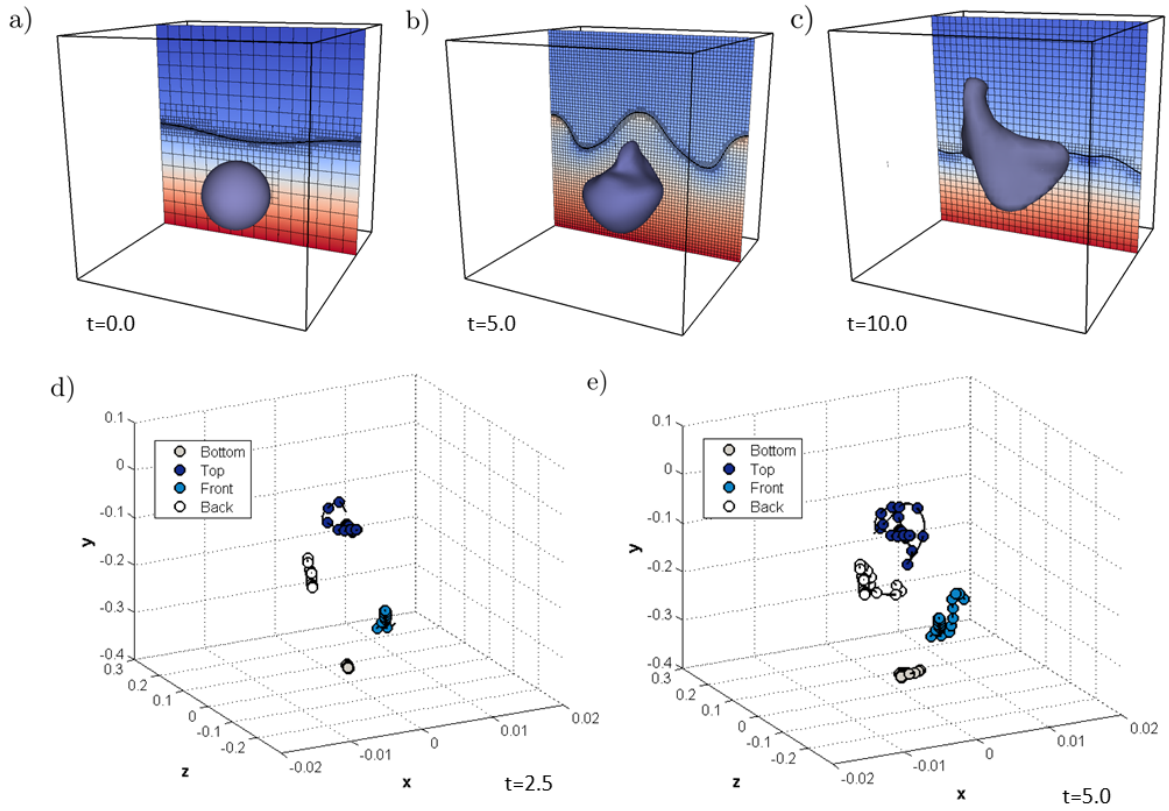

Figure 7: Isosurface of the passive tracer with a value equal to the target concentration shown at, a) $t = 0.0$, b) $t = 5.0$, and c) $t = 10.0$, under the action of a symmetric voltage potential distribution; examples of particles originally on the surface of the spherical droplet tracked in the flow at d) $t = 2.5$, and e) $t = 5.0$. The cross-section at $z = 0$ shows the computational mesh and the pressure distribution (red representing high values and blue low ones). An animation of the flow is available as electronic supplementary material.

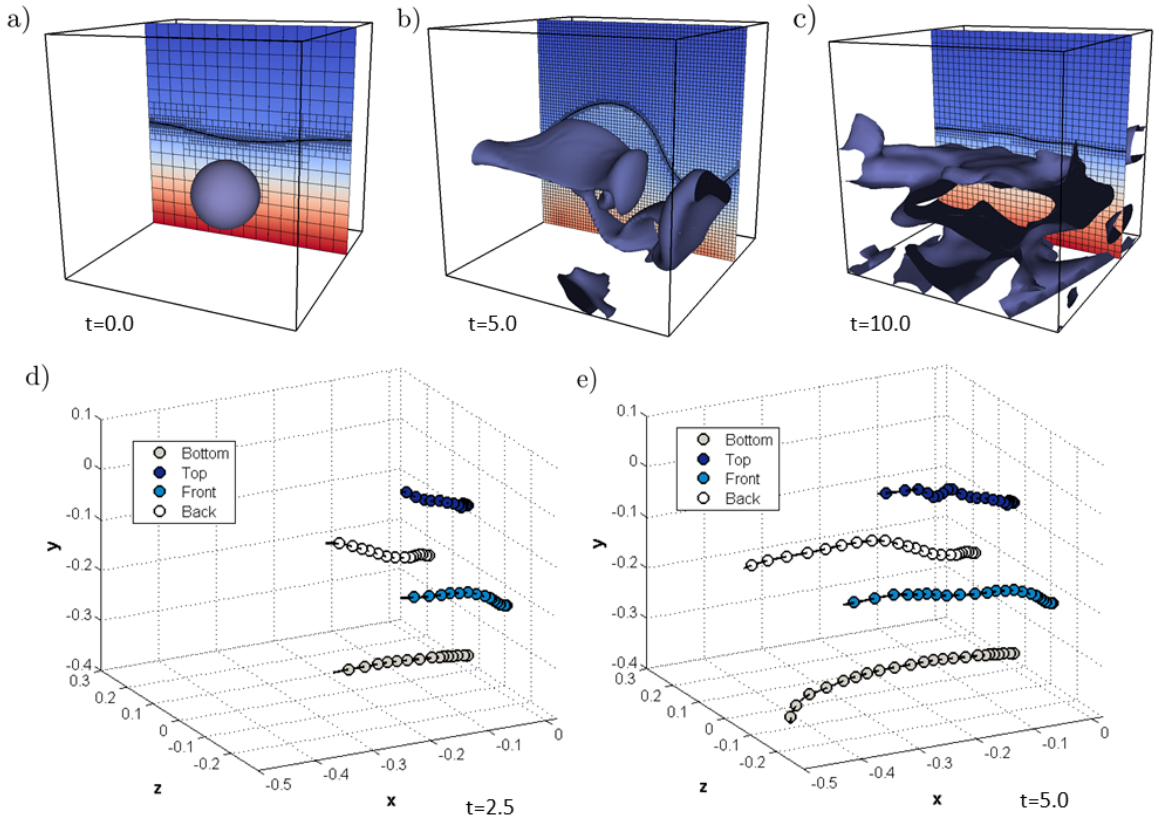

Figure 8: Isosurface of the passive tracer with a value equal to the target concentration shown at, a) $t = 0.0$, b) $t = 5.0$, and c) $t = 10.0$, under the action of an asymmetric voltage potential distribution; examples of particles originally on the surface of the spherical droplet tracked in the flow at d) $t = 2.5$, and e) $t = 5.0$. The cross-section at $z = 0$ shows the computational mesh and the pressure distribution (red representing high values and blue low ones). An animation of the flow is available as electronic supplementary material.

diffusion, however in order to provide a competitive alternative to other active mixers, the inclusion of dielectrophoresis was found to be necessary.

Fig. 8 illustrates the three-dimensional results obtained using the non-uniform voltage potential distribution (29). In this case, particles are steered towards the negative $x-$direction, as can be observed in subfigures (d) and (e). The distance covered by the particles over a similar amount of time as in the results of Fig. 7 is visibly improved (consult values on the $x-$axis), and subfigures (a)-(c) depict more complex trajectories, both in terms of spread as well as the topology of the considered isosurface. The mixing index as described in equation (27), reveals an increase of up to 0.83 in this case. A similar calculation for the uniform voltage distribution shown in Fig. 7 produces a mixing index of approximately 0.47, thus reinforcing the crucial role of the dielectrophoretic effects on mixing.

The computational results presented here provide strong quantitative evidence of the feasibility of electrostatically induced mixing in multi fluid systems; further optimization is likely to generate results that are even better with high mixing indexes attained at shorter times or with optimal time-dependent voltage distributions. We note that both uniform and non-uniform configurations lead to reasonable degrees of mixing in the domain within short time scales. Our computational results show, however, that there is a notable advantage to introducing asymmetry in the voltage distribution model - mixing indexes can be increased significantly in such cases and this may be useful in applications.

4. Conclusions

This theoretical study has successfully identified efficient mixing mechanisms involving the use of electric fields acting on small-scale flow configurations. Our efforts have been directed towards real physical systems forced by simple on-off protocols and dielectrophoretic techniques; the numerical results indicate promising experimental directions in the investigation of enhancing mixing on the microscale. The proposed approach is based on imposing modulated electric fields across the domain and requires no moving parts or mass inflow into the system. The field induces interfacial instabilities and is shown to be capable (under judicious choices of parameters) of generating and sustaining nonlinear spatiotemporal oscillations. These oscillations in turn underpin the enhanced mixing observed in our computations, and high mixing indexes are shown to be possible. We also note that dielectrophoretic traveling-wave voltage boundary conditions have also been shown to produce pumping by generating nonlinear interfacial traveling waves in otherwise stable and quiescent multi fluid flows - see Cimpeanu and Papageorgiou [5] - thus adding further flexibility in applications. We have examined both two- and three-dimensional flows in a variety of test cases using direct numerical simulations based on the VOF method to fully resolve the dynamics well into the nonlinear regime.

Optimization of the presented methods has so far not been tackled. The possibility to expand

the present work to include more specialized voltage potential distributions, as well as perhaps the inclusion of feedback control into such systems is very attractive and merits further exploration.

Acknowledgement

The work of D.T.P. was supported in part by EPSRC grant EP/K041134/1; R.C. acknowledges a Roth Doctoral Fellowship from the Department of Mathematics, Imperial College London.

References

[1] N. Aubry and I. Glasgow. Enhancement of microfluidic mixing using time pulsing. *Lab Chip*, 3:114–20, 2003.

[2] A. Bagué, D. Fuster, S. Popinet, R. Scardovelli, and S. Zaleski. Instability growth rate of two-phase mixing layers from a linear eigenvalue problem and an initial-value problem. *Phys. Fluids*, 22:092104–1, 2010.

[3] A.A.S. Bhagat, E.T.K. Peterson, and I. Papautsky. A passive planar micromixer with obstructions for mixing at low Reynolds numbers. *J. Micromech. Microeng.*, 17:1017–1024, 2007.

[4] R. Cimpeanu and D.T. Papageorgiou. Electrohydrodynamically induced pumping and mixing of multifluid systems in microchannels. In *4th Micro and Nano Flows Conference, University College London, UK, 7-10 September 2014*, ID10, 2014.

[5] R. Cimpeanu and D.T. Papageorgiou. On the generation of nonlinear travelling waves in confined geometry using electric fields. *Phil. Trans. Royal Society A*, 28:20140066, 2014.

[6] R. Cimpeanu, D.T. Papageorgiou, and P.G. Petropoulos. On the control and suppression of the Rayleigh-Taylor instability using electric fields. *Phys. Fluids*, 26:022105–1, 2014.

[7] D.T. Conroy, O.K. Matar, R.V. Craster, and D.T. Papageorgiou. Breakup of an electrified, perfectly conducting, viscous thread in an AC field. *Phys. Rev. E*, 83:066314, 2011.

[8] R.V. Craster and O.K. Matar. Dynamics and stability of thin liquid films. *Rev. Mod. Phys.*, 81:1131, 2009.

[9] P.S. Denkova, S. Tcholakova, N.D. Denkov, K.D. Danov, B. Campbell, C. Shawl, and D. Kim. Evaluation of the Precision of Drop-Size Determination in Oil/Water Emulsions by Low-Resolution NMR Spectroscopy. *Langmuir*, 20:11402–11413, 2004.

[10] T.A. Franke and A. Wixforth. Microfluidics for Miniaturized Laboratories on a Chip. *ChemPhysChem*, 9:2140–2156, 2008.

[11] A. Goullet, I. Glasgow, and N. Aubry. Dynamics of microfluidic mixing using time pulsing. *Discrete and Continuous Dynamical Systems: Supplement Vol.*, pages 327–336, 2005.

[12] V. Hessel, H. Löwe, and F. Schönfeld. Micromixers - a review on passive and active mixing principles. *Chemical Engineering Science*, 60:2479–2501, 2005.

[13] M. Holz, S.R. Heil, and A. Sacco. Temperature-dependent self-diffusion coefficients of water and six selected molecular liquids for calibration in accurate H NMR PFG measurements. *PCCP*, 2:4740–4742, 2000.

[14] S. Hossain and K.-Y. Kim. Mixing analysis of passive micromixer with unbalanced three-split rhombic sub-channels. *Micromachines*, 5:913–928, 2014.

[15] B. Jha, L. Cueto-Felgueroso, and R. Juanes. Fluid mixing from viscous fingering. *Phys. Rev. Lett.*, 106:194502, 2011.

[16] C.-Y. Lee, C.-L. Chang, Y.-N. Wang, and L.-M. Fu. Microfluidic mixing:A review. *Int. J. Mol. Sci.*, 12:3263–3287, 2011.

[17] F. Li, O. Ozen, N. Aubry, D.T. Papageorgiou, and P.G. Petropoulos. Linear stability of a two-fluid interface for electrohydrodynamic mixing in a channel. *J. Fluid Mech.*, 583:347, 2007.

[18] J.M. López-Herrera, S. Popinet, and M.A. Herrada. A charge-conservative approach for simulating electrohydrodynamic two-phase flows using volume-of-fluid. *J. Comput. Phys.*, 230:1939–1955, 2011.

[19] J.R. Melcher. Electrohydrodynamic and magnetohydrodynamic surface waves and instability. *Phys. Fluids*, 4:1348–1354, 1961.

[20] J.R. Melcher. *Field-Coupled Surface Waves*. Technology Press, Cambridge, Massachusetts, 1963.

[21] J.R. Melcher and E.P. Warren. Continuum feedback control of a Rayleigh-Taylor type instability. *Phys. Fluids*, 9:2085–2094, 1966.

[22] A.O. El Moctar, N. Aubry, and J. Batton. Electro-hydrodynamic micro-fluidic mixer. *Lab Chip*, 3:273–280, 2003.

[23] J.M. Ottino and S. Wiggins. Introduction: mixing in microfluidics. *Phil. Trans. Royal Society A*, 362(1818):923–935, 2004.

[24] O. Ozen, N. Aubry, D.T. Papageorgiou, and P.G. Petropoulos. Electrohydrodynamic linear stability of two immiscible fluids in channel flow. *Electrochimica Acta*, 51:5316, 2006.

[25] O. Ozen, N. Aubry, D.T. Papageorgiou, and P.G. Petropoulos. Monodisperse drop formation in square microchannels. *Phys. Rev. Lett.*, 96:144501, 2006.

[26] S. Popinet. Gerris: A tree-based adaptive solver for the incompressible Euler equations in complex geometries. *J. Comput. Phys.*, 190:572, 2003.

[27] L. Rayleigh. Investigation of the character of the equilibrium of an incompressible heavy fluid of variable density. *Proc. London Math. Soc.*, 14:170, 1883.

[28] S. A. Roberts and S. Kumar. Electrohydrodynamic instabilities in thin liquid trilayer films. *Physics of Fluids (1994-present)*, 22(12), 2010.

[29] S.A. Roberts and S. Kumar. AC electrohydrodynamic instabilities in thin liquid films. *J. Fluid Mech.*, 631:255–279, 2009.

[30] D.A. Saville. Electrohydrodynamics: The Taylor-Melcher leaky dielectric model. *Annu. Rev. Fluid Mech.*, 29:27, 1997.

[31] E. Schäffer, T. Thurn-Albrecht, and T.P. Russell. Electrically induced structure formation and pattern transfer. *Nature*, 403:874–877, 2000.

[32] P. Singh and N. Aubry. Transport and deformation of droplets in a microdevice using dielectrophoresis. *Electrophoresis*, 28(4):644–657, 2007.

[33] H.A. Stone, A.D. Stroock, and A. Ajdari. Engineering flows in small devices. Microfluidics toward a lab-on-a-chip. *Annu. Rev. Fluid Mech.*, 36:381, 2004.

[34] Y.K. Suh and S. Kang. A Review on Mixing in Microfluidics. *Micromachines*, 1(3):82–111, 2010.

[35] G.I. Taylor. The instability of liquid surfaces when accelerated in a direction perpendicular to their planes. I. *Proc. R. Soc. London, Ser. A*, 201:192, 1950.

[36] G.I. Taylor and A.D. McEwan. The stability of a horizontal fluid interface in a vertical electric field. *J. Fluid Mech.*, 22:1–15, 1966.

[37] J.-L. Thiffeault. Using multiscale norms to quantify mixing and transport. *Nonlinearity*, 25(2):R1, 2012.

[38] G. Tomar, D. Gerlach, G. Biswas, N. Alleborn, A. Sharma, F. Durst, S.W.J. Welch, and A. Delgado. Two-phase electrohydrodynamic simulations using a volume-of-fluid approach. *J. Comput. Phys.*, 227-2:1267, 2007.

[39] C. Tsouris, C.T. Culbertson, D.W. DePaoli, S.C. Jacobson, V.F. de Almeida, and J.M. Ramsey. Electrohydrodynamic Mixing in Microchannels. *Al. Ch. E.*, 49:8:2181–2186, 2003.

[40] C.-T. Wang, Y.-C. Hu, and T.-Y. Hu. Biophysical Micromixer. *Sensors*, 9:5379–5389, 2009.

[41] Y.L. Yeo, R.V. Craster, and O.K. Matar. Drop manipulation and surgery using electric fields. *J. Colloid Interface Sci.*, 306:368–378, 2007.

[42] J.D. Zahn and V. Reddy. Two phase micromixing and analysis using electrohydrodynamic instabilities. *Microfluid Nanofluid*, 2:399–415, 2006.